Electroluminescence of negatively charged single NV centers in diamond

Cite as: Appl. Phys. Lett. **122**, 072101 (2023); doi: 10.1063/5.0138050
Submitted: 21 October 2022 · Accepted: 31 January 2023 ·
Published Online: 14 February 2023

M. Haruyama,[1,a)] H. Kato,[1] M. Ogura,[1] Y. Kato,[1] D. Takeuchi,[1] S. Yamasaki,[1,2] T. Iwasaki,[3] H. Morishita,[4,5] M. Fujiwara,[4] N. Mizuochi,[4,5] and T. Makino[1]

AFFILIATIONS

[1]Advanced Power Electronics Research Center, National Institute of Advanced Industrial Science and Technology, Umezono, Tsukuba, Ibaraki 305-8568, Japan
[2]Nanomaterials Research Institute, Kanazawa University, Kanazawa, Ishikawa 920-1192, Japan
[3]Department of Electrical and Electronics Engineering, School of Engineering, Tokyo Institute of Technology, Ookayama, Meguro, Tokyo 152-8552, Japan
[4]Institute for Chemical Research, Kyoto University, Gokasho, Uji, Kyoto 611-0011, Japan
[5]Center for Spintronics Research Network, Institute for Chemical Research, Kyoto University, Gokasho, Uji, Kyoto 611-0011, Japan

[a)]Author to whom correspondence should be addressed: haruyama.moriyoshi@aist.go.jp

ABSTRACT

The realization of electroluminescence (EL) of negatively charged nitrogen vacancy (NV^-) centers is important toward all-electrical control of diamond quantum devices. In this study, we demonstrated electrical excitation and detection of EL of single NV^- centers by using lateral diamond p^+–i(n^-)–n^+ diodes. It had been grown by homoepitaxy using the plasma enhanced chemical vapor deposition technique. We introduced a lightly phosphorus doped i(n^-) layer to stabilize the negative state of NV centers. It was estimated that the efficiency of the electrical excitation rate of the NV center was more than 30 times enhanced by introducing lateral diamond p^+–i(n^-)–n^+ diodes structure compared with the previous vertical diode. Furthermore, the EL of a single NV^- center embedded in the i(n^-) layer region was characterized. The results show that the charge state of the single NV centers can be manipulated by the voltage applied to the p^+–i(n^-)–n^+ diode, where the emission of EL is increasingly dominated by NV^- in the range of 30 to 50 V.

© *2023 Author(s). All article content, except where otherwise noted, is licensed under a Creative Commons Attribution (CC BY) license (http://creativecommons.org/licenses/by/4.0/).* https://doi.org/10.1063/5.0138050

Negatively charged nitrogen vacancy (NV^-) centers are expected to be useful for various quantum devices.[1,2] Because NV^- centers have a long coherence time at room temperature,[3–8] they are expected to be useful for quantum sensing, quantum networks,[9–11] quantum information processing,[12–14] and so on. Especially in recent years, there has been much research on quantum sensing. For example, magnetocardiography of living rats,[15] electrical field sensing in diamond devices,[16] temperature sensing of living cells,[17] and pH sensors[18] have been proposed. A prototype of a handheld magnetometer using NV centers was developed.[19] One of the advantages of NV centers is initialization and readout of the electron spin state by laser irradiation. On the other hand, objective lenses, excitation lasers, photodetectors, etc., prevent the integration of quantum devices. Electrical excitation and readout[20–23] without an optical system were required for the integration of quantum sensor, quantum register, quantum repeater, and any quantum devices.

Previously, research works on electrical excitation of single NV centers and silicon-vacancy center ensembles by using a pin diode were reported.[24–26] In the previous report, electroluminescence (EL) of a single NV center by using a vertical p^+–i–n^+ diode was achieved.[24] We grew the i layer and phosphorus doped n type layer by the plasma enhanced chemical vapor deposition (PECVD) method on (001) high-pressure high-temperature (HPHT) IIb p type substrate. From EL spectrum and photon-antibunching measurements, electrical excitation of a single NV^0 center was achieved. Lohrmann *et al.* reported EL of a single NV center by using a lateral pin diode.[25] They implanted phosphorus and boron ions into (001) diamond grown by plasma enhanced chemical vapor deposition (PECVD) technique and demonstrated EL of a single NV^0 center. With implantation technology for the doping of diamond, in general, it is known that various non-intended defects are formed, preventing the production of n-type diamond characterized by Hall measurement. A technologically relevant

© Author(s) 2023

device that emits EL from negatively charged single NV centers is, therefore, still missing.

Electrical excitation of NV^- centers is required for the integration of quantum devices. Over the past decade, various stabilization methods have been proposed. One of the approaches was charge state control of NV centers by using a PIN or Schottky diode.[27,28] The charge state of NV^- centers can be excitation stabilized by applying a reverse bias voltage. In another approach, the charge state of NV^- centers can be stabilized by controlling the Fermi level using a phosphorus doped n type layer[29] or i layer in a negative–intrinsic–negative structure.[30] Especially for the n type layer, over 99% of the NV center charge state was negatively stabilized.[29] Furthermore, phosphorus doping has a positive effect of prolonging spin coherence times at appropriate concentrations.[6]

In this paper, we report the use of a lateral p^+–i(n^-)–n^+ diode arrangement with a lightly phosphorus doped i(n^-) layer to stabilize the negative charge state of NV centers and heavily phosphorus doped n^+ contact for higher electron injection. A series of p^+–i(n^-)–n^+ structures have been prepared to optimize diode properties with respect to quantum applications. The detection of EL spectra was maximized in these lateral p^+–i(n^-)–n^+ diodes as the shading effects due to contacts could be prevented, and additional luminescence from the n^+ layer could be minimized.

A top view of a lateral p^+–i(n^-)–n^+ diode measured by optical microscope is shown in Fig. 1(a), and a cross-sectional view of the diode is shown in Fig. 1(b). The intrinsic layer was grown on (111) lb HPHT substrate by using the PECVD method. The i(n^-) layer was lightly doped with phosphorus (P concentration: $10^{16}\,cm^{-3}$) to stabilize the charge state of NV^- centers. Boron doped p^+ (B concentration: $10^{20}\,cm^{-3}$) and phosphorus doped n^+ (P concentration: $10^{20}\,cm^{-3}$) layers were selectively grown on the i(n^-) layer by PECVD through patterned metal mask, which were formed by photolithography and the liftoff process. The respective thicknesses of the p^+ and n^+ layers were several hundred nm. The width between the p^+ and n^+ layers was $\sim$7 μm. NV centers were created by using nitrogen (N) ion implantation techniques. ^{14}N ion was implanted to the whole of the sample with the energy of 350 keV at 600 °C. Ion fluence was $5 \times 10^8\,cm^{-2}$. Implantation depth was calculated to be 340 nm by Stopping and Range Ion in Matter (SRIM).[31] After ion implantation, annealing was performed at 850 °C for 30 min in Ar to diffuse vacancies and create NV centers. After annealing, boiled acid mixture treatment (H_2SO_4 and HNO_3) was performed to terminate the surface with oxygen. Electrodes (Ti/Pt/Au) were created on both the p^+ and n^+ layers. NV centers were observed by using a confocal laser scanning fluorescence microscope (CFM). The excitation laser was a 532 nm diode pumped solid state laser. The laser was irradiated via an oil immersion objective lens (numerical aperture: 1.42 and magnification: 60×). Photoluminescence (PL) and EL of NV centers were corrected by an avalanche photodiode and spectrometer through a 30 μm diameter pinhole and long-pass filter (LPF).

Figure 1(d) shows the current–voltage (I–V) curve of the fabricated lateral p^+–i(n^-)–n^+ diode. The I–V curve was obtained by using a semiconductor parameter analyzer (Keithley 4200A). The measurement was performed under the same conditions as EL measurement, and a voltage was applied via gold wire in the atmosphere with immersion oil. Rectification characteristics over four orders of magnitude were observed. Leakage current was suppressed in vacuum, and a higher rectification characteristic over seven orders of magnitude was observed. The typical threshold voltage of a diamond p^+–i(n^-)–n^+ diode, between 4 and 5 V, was observed. Typical diode characteristics were obtained by I–V measurement.

Figure 2 shows CFM maps [(a) and (b)] and luminescence spectra [(c) and (d)]. In PL CFM map [Fig. 2(a)], luminescence of NV centers was detected via 633 nm LPF to suppress the excitation laser light and Raman scattering of diamond. The PL spectrum and all EL measurements [Figs. 2(b)–2(d)] were obtained by using 561 nm LPF. These EL measurements were performed under an applied forward bias of 30 V and laser-off. The current was 0.4 mA in this condition. Figures 2(a) and 2(b) show PL and EL CFM maps for the same region. The upper, middle, and lower regions in these figures show the p^+ layer, i(n^-) layer, and n^+ layer, respectively. As shown in these figures, isolated luminescence centers were observed at the p^+ and i(n^-) layers. In both PL and EL at the n^+ region, bright luminescence was observed.

Figures 2(c) and 2(d) show PL and EL spectra of luminescence centers in the i(n^-) layer. The luminescence spectrum at the

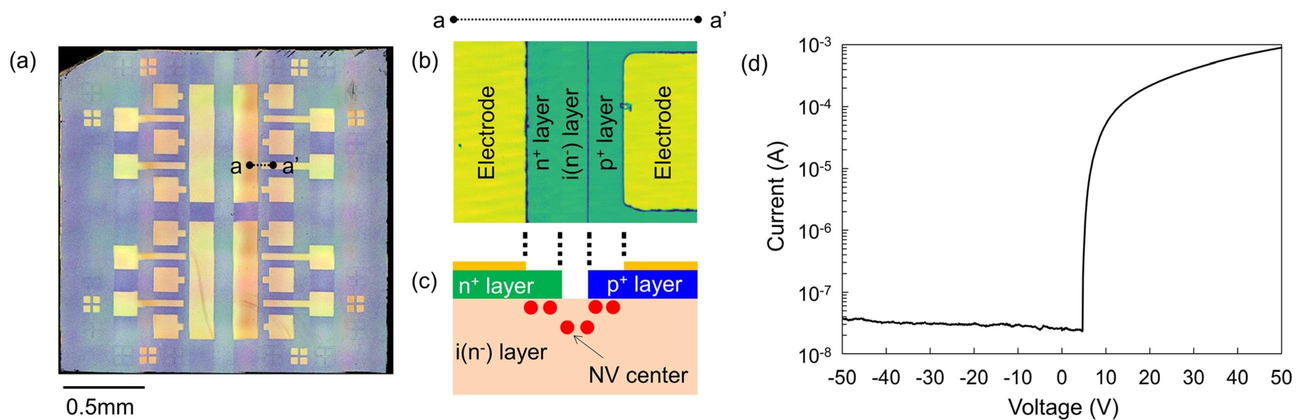

FIG. 1. (a) Optical microscope image of lateral p^+–i(n^-)–n^+ diodes in PECVD diamond. (b) Magnified optical microscope image of the lateral p^+–i(n^-)–n^+ diode used in this study. (c) Cross-sectional image of lateral p^+–i(n^-)–n^+ diode. (d) I–V measurement result of lateral p^+–i(n^-)–n^+ diode.

© Author(s) 2023

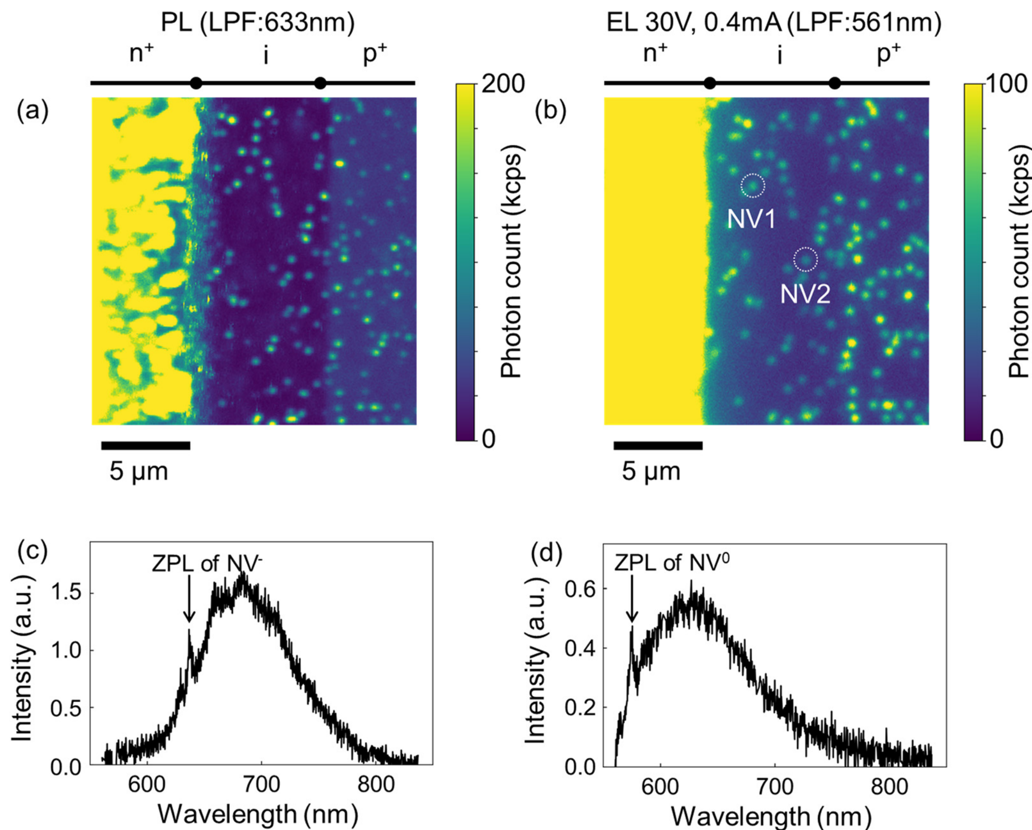

FIG. 2. (a) PL CFM map. (b) EL CFM map. Applied forward bias was 30 V, and current was 0.4 mA. Broken circles "NV1" and "NV2" indicated the single NV centers analyzed in Figs. 3 and 4, respectively. (c) PL spectrum of a single NV center in the i(n^-) layer. (d) EL spectrum of a single NV center in the i(n^-) layer.

background position, which measured several micrometers distant from the NV center in the horizontal direction, was subtracted from both the PL and EL spectra. As shown in Fig. 2(c), because zero-phonon line (ZPL) at 637 nm and the typical phonon sidebands of the NV^- center were observed,[32] the origin of the luminescence center was assigned to the NV^- center. Figure 2(d) shows the EL spectrum of luminescence centers. As seen from this spectrum, the luminescence spectrum originated from the NV^0 center because ZPL at 575 nm and the typical phonon sidebands of the NV^0 center were observed.

Figures 3(a) and 3(b) show PL and EL photon-antibunching of NV centers. The solid gray line and solid black line represent the background corrected autocorrelation function $g^{(2)}(\tau)$ and fitting curve, respectively.[33] As shown in Fig. 3(a), typical photon-antibunching of NV^- centers was obtained. We used a three-level model fitting function, $g^{(2)}(\tau) = 1 - (1 + a_1)\exp(-|\tau|/\tau_1) + a_2\exp(-|\tau|/\tau_2)$, where a_1 and a_2 are contrasts, τ_1 is the lifetime from the first excited triplet state to the ground triplet state, and τ_2 is the lifetime of the singlet shelving state in the three levels model.[33] They were estimated to be $\tau_1 = 7.7 \pm 0.1$ ns and $\tau_2 = 229.3 \pm 1.6$ ns, which were typical values for NV^- centers.[33] Because $g^{(2)}(0) < 0.5$, we conclude that the PL originated from the single NV center.

Figure 3(b) shows EL antibunching from NV centers. In the previous research,[24] it was revealed that the generation of electroluminescence of the NV^0 center follows fundamentally different kinetics than photoluminescence with intra-bandgap excitation. The differences appear in the slow decay of $g^{(2)}(\tau)$ and the decay shape of $g^{(2)}(\tau)$ close to $\tau = 0$, as shown in Fig. 3(b). We used the three-level model fitting function, $g^{(2)}(\tau) = 1 + a_3\exp(\lambda|\tau|) + a_4\exp(\gamma|\tau|)$, where a_3 and a_4 are contrasts. The parameters of λ and γ were derived by solving a rate equation with the rates among the three levels in previous research as shown in Fig. 3(c).[24] Schematic diagram of the dynamics was shown in Fig. 3(c). Levels 1, 2, and 3 were corresponding to ground state, excited state, and electrical pumping state of NV^0 center. The rates among the states of k_{13}, k_{32}, and k_{21} are taken into account in the analysis, and these are depicted in Fig. 3(c). It should be noted that k_{13} is the electrical excitation rate from state 1 to state 3, and $1/k_{21}$ is the lifetime of the NV^0. Similar to the previous research,[6] $1/k_{21} = 13.2$ ns and $1/k_{32} = 266$ ns were used and kept constant for the simulation of $g^{(2)}(\tau)$. The simulated $g^{(2)}(\tau)$ with an adjustable parameter k_{13} and constants of k_{21} and k_{32} were fitted well to the experimental data. The EL originated from a single NV center because $g^{(2)}(0) < 0.5$. Therefore, we conclude that EL of a single NV center is demonstrated by using the lateral p^+–i(n^-)–n^+ diode fabricated in this study. The $g^{(2)}(0)$ was estimated to be 0.02, so fluorescence intensity other than the single NV center is very small in our measurement after subtracting the background.

The electrical excitation rate k_{13} was estimated to be 0.045 ns^{-1} from the well reproduced $g^{(2)}(\tau)$ in Fig. 3(b). It was revealed that the

© Author(s) 2023

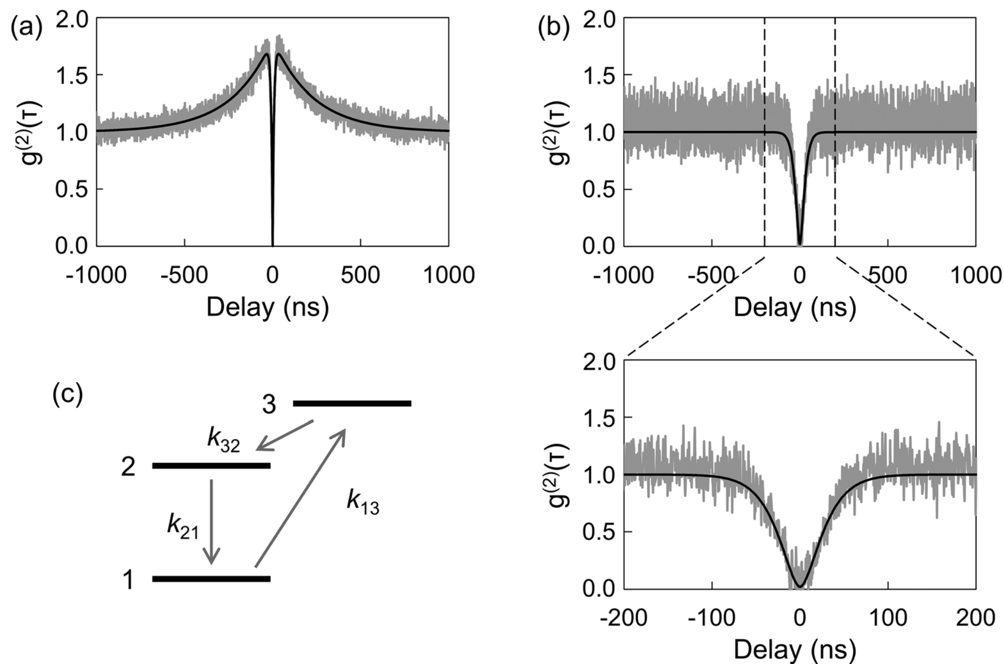

FIG. 3. (a) PL antibunching. The solid gray line and solid black line represent raw data and fitting curve, respectively. (b) EL antibunching. The solid gray line and solid black line represent raw data and fitting curve, respectively. The downside of (b) shows magnified EL antibunching between −200 and 200 ns. (c) Schematic diagram of dynamics of electroluminescence. Levels 1, 2, and 3 were corresponding to ground state, excited state, and electrical pumping state of NV^0 center, respectively. k_{13}, k_{32}, and k_{21} were transition rate among each state.

k_{13} depends almost linearly on the amount of the injected current, and the larger the current, the faster the rate, as shown previously.[24] By comparing k_{13}, the rate of 0.045 ns^{-1} with the injected current of 0.4 mA in the present study almost corresponds to that with the injected current of 12.4 mA in the previous research. This indicates that the electrical excitation of the NV center is about 31 times more efficient than the previous one by introducing the lateral structure in the present study. It should be noted that the current values shown in this study and previous experiments were the total amount of current flowing the p^+–i(n^-)–n^+ diode, and local current around the observed NV center contributes to the electrical excitation. For a more detailed discussion of the electrical excitation efficiency, it was necessary to consider the current inhomogeneity depending on local electric field and the excitation location between the p^+ layer side and the n^+ layer side.

Next, we evaluated the voltage dependence of the EL spectrum from the single NV center. We measured the EL spectrum by changing the applied forward bias to 10, 30, and 50 V, at which voltages the current was 0.06, 0.4, and 0.8 mA, respectively. ZPL of the NV^0 center (575 nm) was observed in all spectra. Luminescence without NV centers was not included in these spectra because the observed NV centers were shown to be single one by EL photon-antibunching measurement. It is known that the charge state of NV centers can stochastically change during laser irradiations.[34] It is considered that the origin of the luminescence from these EL spectra was the NV^0 center or NV^- center. To estimate the amount of luminescence other than the NV^0 center, the NV^0 component was subtracted from each spectrum. The amount of the NV^0 component for subtraction was normalized at the ZPL intensity of the NV^0 center. The subtracted spectrum is considered to be the difference of the NV^- component in each spectrum for the different applied voltages. Figure 4(a) shows normalized EL spectra with an applied forward bias of 10 V, 30 V, and subtracted spectra, which are denoted by S_{10V}, S_{30V}, and $\Delta S_{30V,10V}$, respectively. The solid green line, solid light blue line, and solid red line corresponded to S_{10V}, S_{30V}, and $\Delta S_{30V,10V}$, respectively. As shown by $\Delta S_{30V,10V}$, a clear luminescence peak was not observed. It indicates that the EL from the NV^- center did not differ when the applied forward bias was changed from 10 to 30 V. Figure 4(b) shows normalized EL spectra when the applied forward bias was 30 V, 50 V, and subtracted spectra, which are denoted by S_{30V}, S_{50V}, and $\Delta S_{50V,30V}$, respectively. The EL spectrum at 30 V in this figure was the same data as S_{30V} in Fig. 4(a). The solid light blue line, solid blue line, and solid red line corresponded to S_{30V}, S_{50V}, and $\Delta S_{50V,30V}$, respectively. As shown in $\Delta S_{50V,30V}$, broad luminescence was observed. Yellow solid line shows typical photoluminescence spectrum of single NV^- center. The subtracted spectrum of $\Delta S_{50V,30V}$ was in good agreement with the spectrum of the NV^- center, so it is considered that this luminescence corresponded to the NV^- component. Therefore, the NV^- component differed depending on the applied forward bias. The NV^- component increased as the applied forward bias was increased from 30 to 50 V. We conclude that EL from NV^- centers was observed by using the lateral p^+–i(n^-)–n^+ diode.

One of the reasons why EL of NV^- centers was observed in this study was considered to be the charge stabilization effect of the lightly phosphorus doped i(n^-) layer. As noted earlier, it is well known that the charge state of NV centers in the i(n^-) layer is negatively stabilized. In the previous study, the *i* layer was not intentionally doped with any impurities, which probably made the Fermi level deep.[24] On the other hand,

© Author(s) 2023

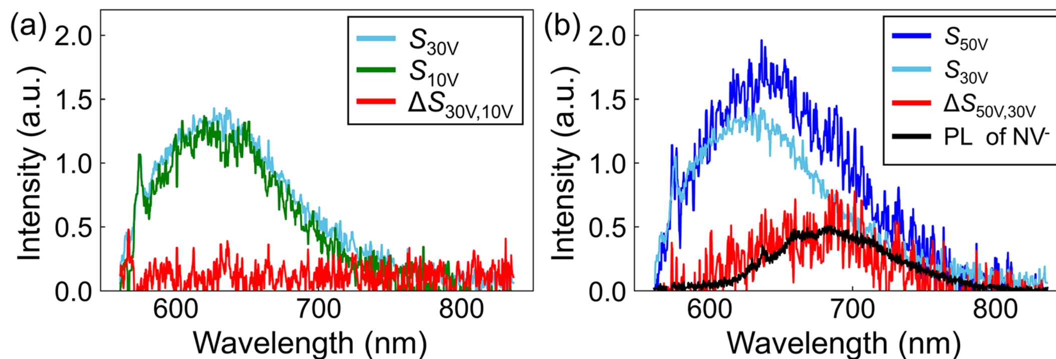

FIG. 4. (a) EL spectra with applied forward bias of 10 V, 30 V, and subtraction of these spectra, denoted by S_{10V}, S_{30V}, and $\Delta S_{30V,10V}$, respectively. The solid orange line, solid green line, and solid red line correspond to S_{10V}, S_{30V}, and $\Delta S_{30V,10V}$, respectively. (b) EL spectra with applied forward bias of 30 V, 50 V, and subtraction of these spectra. The EL spectrum at 50 V and subtracted spectrum are denoted by S_{50V} and $\Delta S_{50V,30V}$, respectively. The EL spectrum at 30 V in this figure was the same data as S_{30V} in (a). The solid green line, solid blue line, and solid red line correspond to S_{30V}, S_{50V}, and $\Delta S_{50V,30V}$, respectively.

the charge state of NV^- centers was stabilized by using the i(n^-) layer in this study. We confirmed that the NV^- component increased as the applied forward bias was increased from 30 to 50 V. This result suggests that the charge state of NV centers was negatively stabilized because electron injection around NV centers increased with increasing forward bias voltage. In this work, we demonstrated EL of NV^- centers by focusing on a single NV center. Further electrical excitation of highly dense NV^- centers is required in order to improve the sensitivity.

We examined the electrically stimulated emission of negatively charged single NV centers incorporated in a lateral p^+–i(n^-)–n^+ diode arrangement. This diode was fabricated by homoepitaxial growth of diamond using the PECVD technique in combination with gas phase doping to form p^+ and n^+ layers. In addition, a lightly phosphorus doped i(n^-) layer was grown to stabilize the negative charge state of the NV centers. Electrical excitation of NV centers could be detected and analyzed by CFM mapping, luminescence spectroscopy, and photon-antibunching measurements. The voltage-dependent EL spectra were discussed and analyzed by correcting detailed spectra with respect to effects arising from the neutral and negative charge state of the NV centers. We found that the emission contains both NV^0 and NV^- components, while the NV^- component can be enhanced by optimizing the p^+–i(n^-)–n^+ diode structure and applied voltage to increase electron injection.

This work was supported by the MEXT Quantum Leap Flagship Program (MEXT Q-LEAP), under Grant No. JPMXS0118067395, the Collaborative Research Program of Institute for Chemical Research, Kyoto University (2022-72), and the Spintronics Research Network of Japan.

AUTHOR DECLARATIONS

Conflict of Interest

The authors have no conflicts to disclose.

Author Contributions

Moriyoshi Haruyama: Conceptualization (equal); Data curation (equal); Formal analysis (equal); Investigation (equal); Methodology (equal); Validation (equal); Visualization (equal); Writing – original draft (equal); Writing – review & editing (equal). **Norikazu Mizuochi:** Formal analysis (equal); Resources (equal); Writing – original draft (equal); Writing – review & editing (equal). **Toshiharu Makino:** Formal analysis (equal); Methodology (equal); Project administration (equal); Resources (equal); Supervision (equal); Writing – original draft (equal); Writing – review & editing (equal). **Hiromitsu Kato:** Conceptualization (equal); Funding acquisition (equal); Methodology (equal); Project administration (equal); Resources (equal); Supervision (equal); Writing – original draft (equal); Writing – review & editing (equal). **Masahiko Ogura:** Resources (equal); Writing – original draft (equal); Writing – review & editing (equal). **Yukako Kato:** Resources (equal); Writing – original draft (equal); Writing – review & editing (equal). **Daisuke Takeuchi:** Resources (equal); Writing – original draft (equal); Writing – review & editing (equal). **Satoshi Yamasaki:** Writing – original draft (equal); Writing – review & editing (equal). **Takayuki Iwasaki:** Writing – original draft (equal); Writing – review & editing (equal). **Hiroki Morishita:** Resources (equal); Writing – original draft (equal); Writing – review & editing (equal). **Masanori Fujiwara:** Resources (equal); Writing – original draft (equal); Writing – review & editing (equal).

DATA AVAILABILITY

The data that support the findings of this study are available from the corresponding author upon reasonable request.

REFERENCES

[1]A. Gruber, A. Drabenstedt, C. Tietz, L. Fleury, J. Wrachtrup, and C. von Borczyskowski, Science **276**, 2012 (1997).
[2]J. R. Maze, P. L. Stanwix, J. S. Hodges, S. Hong, J. M. Taylor, P. Cappellaro, L. Jiang, M. V. G. Dutt, E. Togan, A. S. Zibrov, A. Yacoby, R. L. Walsworth, and M. D. Lukin, Nature **455**, 644 (2008).
[3]G. Balasubramanian, P. Neumann, D. Twitchen, M. Markham, R. Kolesov, N. Mizuochi, J. Isoya, J. Achard, J. Beck, J. Tissler, V. Jacques, P. R. Hemmer, F. Jelezko, and J. Wrachtrup, Nat. Mater. **8**, 383 (2009).
[4]K. D. Jahnke, B. Naydenov, T. Teraji, S. Koizumi, T. Umeda, J. Isoya, and F. Jelezko, Appl. Phys. Lett. **101**, 012405 (2012).
[5]T. Yamamoto, T. Umeda, K. Watanabe, S. Onoda, M. L. Markham, D. J. Twitchen, B. Naydenov, L. P. McGuinness, T. Teraji, S. Koizumi, F. Dolde, H. Fedder, J. Honert, J. Wrachtrup, T. Ohshima, F. Jelezko, and J. Isoya, Phys. Rev. B **88**, 075206 (2013).

© Author(s) 2023

[6] E. D. Herbschleb, H. Kato, Y. Maruyama, T. Danjo, T. Makino, S. Yamasaki, I. Ohki, K. Hayashi, H. Morishita, M. Fujiwara, and N. Mizuochi, Nat. Commun. **10**, 3766 (2019).
[7] G. Balasubramanian, I. Y. Chan, R. Kolesov, M. Al-Hmoud, J. Tisler, C. Shin, C. Kim, A. Wojcik, P. R. Hemmer, A. Krueger, T. Hanke, A. Leitenstorfer, R. Bratschitsch, F. Jelezko, and J. Wrachtrup, Nature **455**, 648 (2008).
[8] N. Aslam, M. Pfender, P. Neumann, R. Reuter, A. Zappe, F. F. de Oliveira, A. Denisenko, H. Sumiya, S. Onoda, J. Isoya, and J. Wrachtrup, Science **357**, 67 (2017).
[9] W. Pfaff, B. J. Hensen, H. Bernien, S. B. van Dam, M. S. Blok, T. H. Taminiau, M. J. Tiggelman, R. N. Schouten, M. Markham, D. J. Twitchen, and R. Hanson, Science **345**, 532 (2014).
[10] B. Hensen, H. Bernien, A. E. Dréau, A. Reiserer, N. Kalb, M. S. Blok, J. Ruitenberg, R. F. L. Vermeulen, R. N. Schouten, C. Abellán, W. Amaya, V. Pruneri, M. W. Mitchell, M. Markham, D. J. Twitchen, D. Elkouss, S. Wehner, T. H. Taminiau, and R. Hanson, Nature **526**, 682 (2015).
[11] R. Reyes, T. Nakazato, N. Imaike, K. Matsuda, K. Tsurumoto, Y. Sekiguchi, and H. Kosaka, Appl. Phys. Lett. **120**, 194002 (2022).
[12] S. C. Benjamin, D. E. Browne, J. Fitzsimons, and J. J. L. Morton, New J. Phys. **8**, 141 (2006).
[13] F. Dolde, I. Jakobi, B. Naydenov, N. Zhao, S. Pezzagna, C. Trautmann, J. Meijer, P. Neumann, F. Jelezko, and J. Wrachtrup, Nat. Phys. **9**, 139 (2013).
[14] P. Neumann, R. Kolesov, B. Naydenov, J. Beck, F. Rempp, M. Steiner, V. Jacques, G. Balasubramanian, M. L. Markham, D. J. Twitchen, S. Pezzagna, J. Meijer, J. Twamley, F. Jelezko, and J. Wrachtrup, Nat. Phys. **6**, 249 (2010).
[15] K. Arai, A. Kuwahata, D. Nishitani, I. Fujisaki, R. Matsuki, Y. Nishio, Z. Xin, X. Cao, Y. Hatano, S. Onoda, C. Shinei, M. Miyakawa, T. Taniguchi, M. Yamazaki, T. Teraji, T. Ohshima, M. Hatano, M. Sekino, and T. Iwasaki, Commun. Phys. **5**, 200 (2022).
[16] T. Iwasaki, W. Naruki, K. Tahara, T. Makino, H. Kato, M. Ogura, D. Takeuchi, S. Yamasaki, and M. Hatano, ACS Nano **11**, 1238 (2017).
[17] G. Kucsko, P. C. Maurer, N. Y. Yao, M. Kubo, H. J. Noh, P. K. Lo, H. Park, and M. D. Lukin, Nature **500**, 54 (2013).
[18] T. Fujisaku, R. Tanabe, S. Onoda, R. Kubota, T. F. Segawa, F. T.-K. So, T. Ohshima, I. Hamachi, M. Shirakawa, and R. Igarashi, ACS Nano **13**, 11726 (2019).
[19] A. Kuwahata, T. Kitaizumi, K. Saichi, T. Sato, R. Igarashi, T. Ohshima, Y. Masuyama, T. Iwasaki, M. Hatano, F. Jelezko, M. Kusakabe, T. Yatsui, and M. Sekino, Sci. Rep. **10**, 2483 (2020).
[20] E. Bourgeois, A. Jarmola, P. Siyushev, M. Gulka, J. Hruby, F. Jelezko, D. Budker, and M. Nesladek, Nat. Commun. **6**, 8577 (2015).
[21] F. M. Hrubesch, G. Braunbeck, M. Stutzmann, F. Reinhard, and M. S. Brandt, Phys. Rev. Lett. **118**, 037601 (2017).
[22] H. Morishita, S. Kobayashi, M. Fujiwara, H. Kato, T. Makino, S. Yamasaki, and N. Mizuochi, Sci. Rep. **10**, 792 (2020).
[23] T. Murooka, M. Shiigai, Y. Hironaka, T. Tsuji, B. Yang, T. M. Hoang, K. Suda, K. Mizuno, H. Kato, T. Makino, M. Ogura, S. Yamasaki, M. Hatano, and T. Iwasaki, Appl. Phys. Lett. **118**, 253502 (2021).
[24] N. Mizuochi, T. Makino, H. Kato, D. Takeuchi, M. Ogura, H. Okushi, M. Nothaft, P. Neumann, A. Gali, F. Jelezko, J. Wrachtrup, and S. Yamasaki, Nat. Photonics **6**, 299 (2012).
[25] A. Lohrmann, S. Pezzagna, I. Dobrinets, P. Spinicelli, V. Jacques, J.-F. Roch, J. Meijer, and A. M. Zaitsev, Appl. Phys. Lett. **99**, 251106 (2011).
[26] A. M. Berhane, S. Choi, H. Kato, T. Makino, N. Mizuochi, S. Yamasaki, and I. Aharonovich, Appl. Phys. Lett. **106**, 171102 (2015).
[27] H. Kato, M. Wolfer, C. Schreyvogel, M. Kunzer, W. Muller-Sebert, H. Obloh, S. Yamasaki, and C. Nebel, Appl. Phys. Lett. **102**, 151101 (2013).
[28] C. Schreyvogel, M. Wolfer, H. Kato, M. Schreck, and C. E. Nebel, Sci. Rep. **4**, 3634 (2014).
[29] Y. Doi, T. Fukui, H. Kato, T. Makino, S. Yamasaki, T. Tashima, H. Morishita, S. Miwa, F. Jelezko, Y. Suzuki, and N. Mizuochi, Phys. Rev. B **93**, 081203 (2016).
[30] T. Murai, T. Makino, H. Kato, M. Shimizu, T. Murooka, E. D. Herbschleb, Y. Doi, H. Morishita, M. Fujiwara, M. Hatano, S. Yamasaki, and N. Mizuochi, Appl. Phys. Lett. **112**, 111903 (2018).
[31] J. F. Ziegler, M. D. Ziegler, and J. P. Biersack, Nucl. Instrum. Methods Phys. Res., Sect. B **268**, 1818 (2010).
[32] M. W. Doherty, N. B. Manson, P. Delaney, F. Jelezko, J. Wrachtrup, and L. C. L. Hollenberg, Phys. Rep. **528**, 1–45 (2013).
[33] A. Beveratos, S. Kühn, R. Brouri, T. Gacoin, J.-P. Poizat, and P. Grangier, Eur. Phys. J. D **18**, 191 (2002).
[34] N. Aslam *et al.*, New J. Phys. **15**, 013064 (2013).

© Author(s) 2023